Macromolecular Materials and Engineering
www.mme-journal.de

Flaw Sensitivity and Tensile Fatigue of Poly(Vinyl Alcohol) Hydrogels

*William J. Koshut, Caleb Rummel, David Smoot, Alina Kirillova, and Ken Gall**

Tensile fatigue behavior is commonly overlooked as researchers pursue the toughest hydrogels. This work describes a poly(vinyl alcohol) (PVA) hydrogel prepared through freezing–thawing (FT) processing to achieve varied monotonic strength and toughness. The monotonic tensile responses of relatively strong and weak versions of the hydrogel are studied with cylindrical hole and crack-like flaws of different sizes to develop an understanding of monotonic strength in the presence of two different, extreme defect types. The monotonic strength of the samples with cylindrical defects is reasonably predicted using nominal stress which accounts for a loss of load-bearing area, while linear-elastic fracture mechanics gives a first-order approximation of the impact of crack-like flaw size on monotonic strength. A subset of key defected samples are further subjected to cyclic loading and fatigue failure at varying stress amplitude. The cylindrical defect samples outperformed cracked samples in fatigue, and the utilization of four FT cycles instead of two improved both monotonic toughness and fatigue properties. This work represents the first tensile fatigue analysis on defected hydrogel materials, sheds light on the behavior of hydrogels in cyclic loading environments, and evaluates both the monotonic toughness and fatigue behavior of soft materials with and without defects.

1. Introduction

Design and control over the mechanical properties of tissue-like hydrogels have led to a plethora of research for soft materials. Repair or replacement of cartilage, soft tissue engineering, and drug delivery highlight just a few of the extensive applications for this class of materials.[1–4] The onset of opportunities to use hydrogels has introduced a pressing need to understand the long-term behavior of these soft and wet materials for many potential uses in the human body. To ensure a continued wide range of applications, hydrogels must be able to withstand cyclic mechanical loads over prolonged periods of time while still exhibiting functionality and mechanical robustness. In particular, the response of a hydrogel to the existence and growth of various types of flaws either broadens or limits the scope of their applicability. A facile, straightforward synthetic hydrogel with reasonable toughness and structure-property control provides opportunity to understand the impact of flaws on hydrogel mechanical behavior and how improved monotonic toughness potentially translates to improved fatigue performance.

One such model system that allows for the study of how different flaw types impact monotonic and cyclic failure in soft materials is poly(vinyl alcohol) (PVA). This hydrogel system is suitable due to the following factors: adjustable mechanical properties, facile synthetic preparation, biodegradability, biocompatibility, and low toxicity.[5–12] PVA hydrogels can be crosslinked through a FT method allowing for simple preparation of relatively tough hydrogels. This method physically crosslinks the polymer network through microcrystalline domains and imparts intrinsic toughness (area under the stress–strain curve, or resistance to crack propagation) to the hydrogel.[7,13] Through freezing–thawing (FT) cyclic processing of PVA hydrogels, scientists have added another tool to attain high-level control over the mechanical properties of PVA hydrogels. With relative ease-of-processing and structure-property control for a soft material, a PVA hydrogel can be used as a model system to understand the impact of the progression of different kinds of mechanical flaws under monotonic and cyclic loading conditions.

Aiming to understand the early formation of damaging flaws like cracks and cavities in hydrogels, researchers have shifted focus to using synthetic strategies to prevent the creation of cracks and cavities during materials processing. Widespread studies in the realm of developing "flaw-insensitive" or "notch-insensitive" hydrogels have grown recently to prevent catastrophic failure.[14–19] Due to the variable nature of the environment in which they are being used, such as the human body, the specific type of flaw is critical to a material's ability to endure mechanical stresses for two reasons: 1) direct loss of sample area to carry load and 2) amplification of applied stresses to a local region in a material (stress concentration or stress intensity). Cracks and less severe rounded cavities can hinder a soft material from sustaining mechanical loads under both monotonic and cyclic loading conditions. Edge-based cracks present the worst-case scenario due to an intensity of stress at the tip of the crack and exposure to environment. On the other hand, cylindrical holes or notches away from the

W. J. Koshut, C. Rummel, D. Smoot, Dr. A. Kirillova, Prof. K. Gall
Department of Mechanical Engineering and Materials Science
Edmund T. Pratt Jr. School of Engineering
Duke University
Durham, NC 27708, USA
E-mail: kag70@duke.edu

The ORCID identification number(s) for the author(s) of this article can be found under https://doi.org/10.1002/mame.202000679.

DOI: 10.1002/mame.202000679

edge of the material are blunt stress concentrators and are the least detrimental geometrical defects. Several researchers have studied the impact of flaws with regards to the material's sensitivity toward the imposed flaw.[20–24] However, very little has been studied as flaw size increases in materials capable of very large strain deformations.[23] Accounting for the initial growth and subsequent long-term development of these flaws as it relates to strength of a hydrogel is critically important for hydrogels in biomedical applications.

In the deformation and fracture of materials, it is critical to consider the impact of flaws with regard to a material's ability to maintain strength. Various approaches can be used to estimate the impact of flaws on the strength of a material for different flaw geometries and severities such as nominal stress, stress concentration, and stress intensity (fracture mechanics). Nominal stress analysis is simply a reduction in the load-bearing area of a sample due to the presence of a geometric defect. In this highly non-conservative approach, a sample losing a percentage of its area will lose only that same percentage in strength. Nominal stress is a reasonable predictor of strength drop when a soft or low modulus material easily deforms and geometric defects have minimal stress localizing impact. Stress concentration is a quantitative measure of the amplification of local stresses relative to the global applied stresses, and it provides a measure of the local driving force for a specific flaw to propagate or the stability of a flaw at a certain global stress value.[25] Unfortunately, the major issue with using stress concentration approximations for hydrogels comes from the strong link between flaw geometry and stress concentration value. As hydrogels experience large strains, the flaw shape evolves rapidly and typically lowers the stress concentration value. For example, under uniaxial tension, a perfectly circular flaw is quickly turned into an ellipse with its loading axis aligned in the loading direction which has minimal local stress amplification.

Stress intensity factor (fracture mechanics) is used for predictions of the strength of a material with a crack or crack-like flaw based on scaling with the magnitude of local stresses experienced at the tip of the crack.[26] The assumption of this model relies on the tip of the crack coming to a mathematical singularity (crack tip radius of zero) instead of being blunted. Although fracture mechanics has geometrical small strain and deformation limitations akin to stress concentrations, its worst-case scenario assumption about crack tip geometry and stresses can provide some insight into the behavior of cracked soft samples. For soft materials, nominal stress analysis provides an upper bound on strength due to a flaw (smallest possible strength loss for a given flaw size) while fracture mechanics provides a lower bound on strength due to a flaw (greatest possible strength loss for a given flaw size).

The impact of flaws in hydrogels is even less characterized and understood under tensile cyclic loading, where damage can progress and result in sample failure even if a flaw is not "critically" sized. Moreover, tensile testing removes the non-conservative nature of determining failure for samples that can recover from extreme compressive deformation. The progression of flaws under cyclic tensile loading will help to understand one failure mode in hydrogel materials used in load-bearing applications. The common focus on a hydrogel's sensitivity towards the existence and behavior of an initial flaw under monotonic testing is often idealistic since it requires the material to exist in pristine condition, which is practically impossible. In addition, flaw analysis in many "cyclic" papers on hydrogels is commonly halted before completing a large number of cycles or true fatigue failure of a sample is reached. Without sufficient cycles to observe the ultimate failure from longer-term repetitive loads, the hydrogel's resistance to the growth of a flaw has not been truly evaluated over the appropriate range of stress levels. The ultimate goal in this work is to use a PVA hydrogel system with simple preparation and tunable mechanical properties to understand the impact of different flaw types and sizes on cyclic behavior in both high cycle-low stress and low cycle-high stress fatigue.

In this work, PVA hydrogels were prepared with the use of FT cyclic processing as a means to study mechanical behavior of a hydrogel with varied inherent toughness in the presence of cylindrical holes and sharp cracks with systematically increasing size. FT cyclic processing was used to improve monotonic toughness through crystallization of the hydrogel network. Once a chosen FT cyclic process was selected for its enhancement of mechanical properties, attention was turned to the resulting hydrogel's response to different flaw types and dimensions under monotonic loading. This study set out to create the worst-case flaw scenario (sharp crack after FT) and best-case flaw scenario (cylindrical hole before FT). The PVA hydrogel was relatively insensitive to the cylindrical hole type of flaw, but extremely sensitive to the crack-like flaw, despite both of them deforming significantly from their initial geometry on loading. Nominal stress analysis and stress intensity modeling demonstrated how these two flaw types impact the sample strength just within the upper and lower bounds, and thus encompass the impact of flaw type on hydrogel strength. Tensile testing in a cyclic manner was then employed on the PVA hydrogels to study the growth of crack-based flaws and cylindrical hole-based flaws toward ultimate failure of the material. The utilization of additional FT cycles enhanced fatigue behavior in comparing 2 FT cycles to 4 FT cycles. Moreover, samples with sharp crack flaws did not perform as well as those with cylindrical hole flaws for both 2 and 4 FT cycles, in line with decreases in monotonic strength with crack-like flaws. These tensile fatigue results provide a blueprint for analyzing tough but defected hydrogels under long-term, cyclic loading conditions.

2. Results and Discussion

2.1. Chemistry and Sample Geometry

Using methods from prior work,[27] homogenous solutions consisting of PVA (16 wt% with respect to the total weight of deionized water combined with PVA) were obtained with a high degree of processability. The screening process of FT cycles provided a quantitative tracking of the improvement of mechanical properties through crystalline domain development and non-covalent interactions. The synthetic approach utilized in the study is illustrated in **Figure 1**.

A given amount of PVA was combined with deionized water and maintained at 95°C until PVA had fully dissolved for

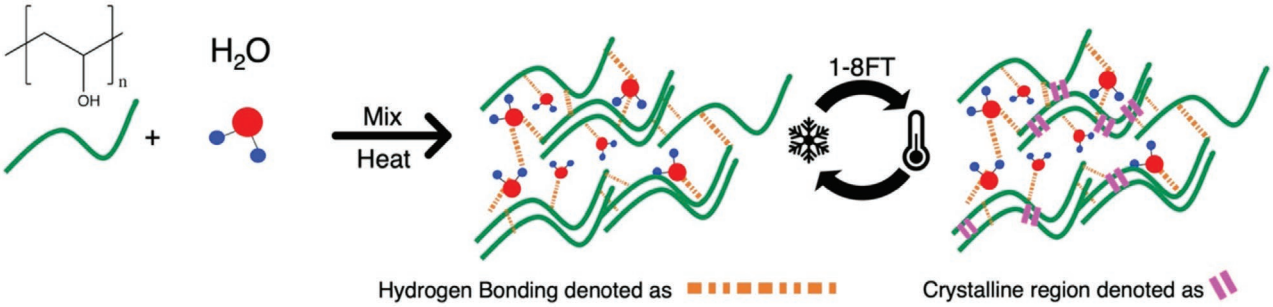

Figure 1. Schematic representation of the PVA-based tough hydrogel preparation strategy using FT cyclic processing.

pouring the solution into the stainless-steel molds. Freezing and subsequent thawing of the samples took place to create the hydrogel. Hydrogen bonding could occur between PVA with itself and PVA with water. Development of crystalline regions was solely attributed to PVA interacting with itself. Representative images of typical monotonic tension samples after final preparation can be seen in **Figure 2**A for the FT cycle screening process, while typical fatigue tension samples can be seen in Figure 2B for samples that had a sharp crack and Figure 2C for samples that had a cylindrical hole.

Adjustment of the shape of the sample was necessary for the following three reasons: 1) the Type V sample had a gauge section that was too small to accommodate larger cracks and cylindrical holes, 2) the Type V samples had a tendency to buckle when tested cyclically in strain-controlled tension, and 3) the Type V-shaped samples had previous issues with failure near the grip section instead of the gauge section when stretched in a cyclic fashion.[27] With these reasons in mind, the same customized fatigue shape previously developed in our work was utilized for fatigue testing herein.[27] This difference in sample geometry of a thicker, shorter gauge section can be seen in comparing Figure 2A to b and c.

Figure 2. Representative optical images of PVA hydrogel samples: A) ASTM D638-14 Type V shape for monotonic tension, B) customized fatigue tension sample for a sharp edge crack, and C) customized fatigue tension sample for a cylindrical hole.

2.2. Screening Process of FT Cycles

Analogous to our prior work,[27] PVA hydrogels were prepared by dissolving the polymer in deionized water and pouring the solution into a designated mold. Subsequently, freezing and thawing the solution was used to physically crosslink the polymer network through crystalline domains, thus creating the hydrogel.[28,29] The starting point of this study took the form of investigating the mechanical properties of the PVA hydrogel by systematically varying the number of FT cycles from one to eight. As opposed to the previous work of utilizing two FT cycles for both control and all bio-friendly toughening agents,[27] this work sought to understand the impact of the number of FT cycles. The hydrogel samples were tested for their monotonic tension properties using the ASTM D638-14 Type V shape to obtain the top-performing FT cycle number based solely on "flaw-free" toughness, which is once again defined as the area under the stress–strain curve. Toughness was selected as the key factor for screening FT cycles due to its practical applications in the realm of soft materials when considering the ability of a hydrogel to dissipate mechanical energy, which is a direct, quantitative relationship to toughness.[30–33]

The goal of the screening process of the FT cycles was to determine a processing cycle number for which toughness was maximized without sacrificing ease-of-processing. **Figure 3**A illustrates the trend for tensile toughness for each FT cycle. Representative tensile stress–strain curves for the PVA samples of differing FT cycles can be seen in Figure 3B.

The toughness values from 1 to 8 FT cycles were: 0.46 MPa ± 0.10 MPa, 1.19 MPa ± 0.35 MPa, 3.38 MPa ± 0.57 MPa, 3.42 MPa ± 0.74 MPa, 3.21 MPa ± 0.72 MPa, 2.47 MPa ± 0.40 MPa, 2.41 MPa ± 0.28 MPa, and 2.37 MPa ± 0.47 MPa. As shown in Figure 3A, the toughness values increased until the maximum at 4 FT cycles, followed by a slow drop off until the toughness values saturated for 6, 7, and 8 FT cycles. This trend in mechanical results can be explained by considering the development, or densification, of crystalline domains of the hydrogel's structure with subsequent FT cycles.[29] As a well-studied physical

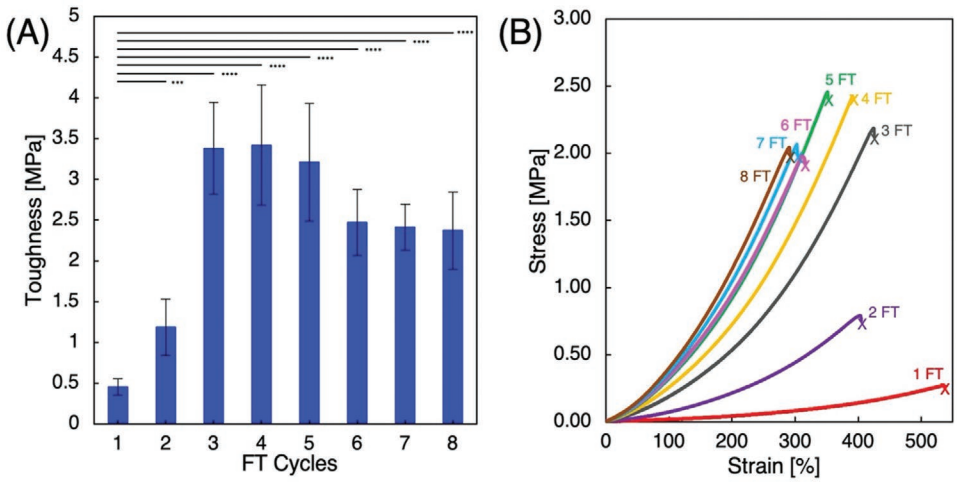

Figure 3. A) Average toughness values for all FT cycles obtained from monotonic tensile stress–strain behavior with ASTM D638-14 Type V shape. Minimum of $n = 9$; data depict mean toughness value ± standard deviation; compared with 1 FT cycle by one-way analysis of variance (ANOVA); $\alpha = 5\%$; * depicts statistical significance in the following manner: $^{*}p < 0.05$; $^{**}p < 0.01$, $^{***}p < 0.001$, $^{****}p < 0.0001$. B) Representative tensile stress–strain behavior of all FT cycles (1 to 8 FT) obtained from monotonic tension testing with ASTM D638-14 Type V shape.

crosslinking strategy, the development of crystalline domains within a hydrogel's network to bear mechanical load is a direct result of FT cyclic processing.[28,29,34] With the onset of additional FT cycles, the size of existing microcrystalline domains grows and new domains can also form.[29] Similar to this work, the densification process of prior work progressed continually for additional FT cycles.[29] By the 6, 7, and 8 FT cycles, a saturation point was reached in this densification process and the toughness values had leveled off. Similar to the trend in toughness, the ultimate tensile strength increased starting from 1 FT until reaching a plateau. Upon leveling off, the ultimate tensile strength dropped for 6, 7, and 8 FT. The strain-to-failure trend can also be explained in terms of densification of the network structure and microcrystalline domains. The highest strain-to-failure values were observed with minimal FT cycles when the microcrystalline domains were not as developed. The lowest strain-to-failure values were obtained with a higher number of FT cycles due to a highly dense network with developed microcrystalline domains.

In order to understand the impact of the FT cycles on the functional properties of the PVA hydrogels, a swelling ratio comparison study was performed. The ability of a hydrogel to uptake water is crucial for potential drug release and tissue engineering applications as well as understanding different stress dissipative mechanisms in articular cartilage and the degree of crosslinking.[35–37] **Figure 4** shows the impact of each FT cycle on the ability of the hydrogel to swell in deionized water at room temperature.

The average swelling ratios were 12.48 ± 0.14, 8.55 ± 0.03, 7.45 ± 0.05, 6.90 ± 0.01, 6.37 ± 0.02, 6.15 ± 0.01, 5.91 ± 0.03, and 5.86 ± 0.02 for each of the FT cycles from one cycle to eight cycles, respectively. In accordance with similar work,[29,38,39] the ability of each FT cycle hydrogel to uptake water decreases with increasing number of FT cycles. This occurs because continually freezing and thawing the hydrogel leads to significant densification of the gel structure with each FT cycle and an overall increase in effective crosslinking density.[29] Additional FT cycles restrict the movement of PVA chains, making it much more difficult for water molecules to penetrate into the polymer chain network.[40] In observing the shift in the swelling capability of the hydrogel-based on FT cycles, the next portion of this study sought to understand the physical impacts in terms of crystallinity on hydrogel structure and network interactions.

2.3. Crystallinity Analysis of FT Cycles

Phase separation of PVA with water, intramolecular hydrogen bonding (PVA with itself), and intermolecular hydrogen

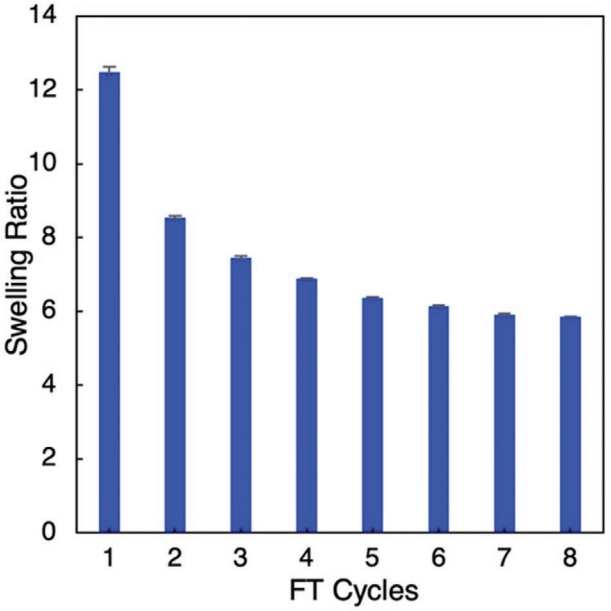

Figure 4. Swelling ratio comparison of all FT cycles using tensile testing samples; data depict mean swelling ratio ± standard deviation.

bonding (PVA with water) were identified as non-covalent molecular interactions in this system.[29] These interactions ultimately paved the way for physical crosslinking of the network structure from the FT cyclic processing steps. It became critical to understand the connection of each FT cycle on the degree of crystallinity in a quantitative manner. The crystallinity of samples from their as-prepared state is subject to change if samples experience an aging or a drying process.[13,41] These aging or drying changes can also impact the functional properties of the hydrogel such as its swelling and mechanical behavior.[42,43] As a result, the analysis of the degree of crystallinity would need to preserve the hydrogel in its as-prepared state to avoid any drying or aging process. In preventing a drying or aging process from occurring, the role of the FT cyclic process could be clearly understood as it relates to any alterations in the crystalline nature of the hydrogel. With these considerations in view, some of the common characterization techniques, such as X-ray diffraction, scanning electron microscopy, and atomic force microscopy, could not be utilized due to concerns of an aging or drying process taking place during analysis. As a result, differential scanning calorimetry (DSC) was employed to characterize the impact of FT cycles on the degree of crystallinity in the as-prepared state.

The amorphous network structure of the PVA hydrogel is comprised of tiny, highly ordered regions of PVA chains that form "knots" as a result of freezing at very cold temperatures.[44] These "knots", or microcrystallites, form as a result of reduced molecular motion for the chains of PVA at low temperature.[45] As PVA chains remained locked in close proximity to one another with the freezing of water, they can interact favorably to create microcrystallite pockets that are physically crosslinked sites for bearing mechanical load. Formation of the "knots" continues to progress with additional freezing and thawing cycles.[28,46,47] Utilizing the endothermic melting of PVA crystallites, the crystallinity degree of a hydrogel sample can be obtained.[41] The crystallinity degree ($\chi_{\%}$) of the hydrogels was calculated using Equation (1)

$$\chi_{\%} = \frac{\Delta H}{\Delta H^{\circ} \times W_{\mathrm{PVA}}} \times 100 \quad (1)$$

where ΔH was calculated as the area under the endothermic melting peak, H° is the heat needed to melt PVA that is 100% crystalline (138.6 J g^{-1}), and W_{PVA} is weight fraction of the PVA polymer in the hydrogel sample with respect to deionized water.[48–50] Figure S1, Supporting Information, provides representative DSC curves from the first heating DSC cycle from which the crystallinity degree was calculated. **Figure 5** provides a view of the trend of crystallinity degree versus an increasing number of FT cycles.

Crystallinity values from 1 to 8 FT were the following: 17.08% ± 2.91%, 29.17% ± 4.74%, 36.86% ± 3.63%, 38.39% ± 4.75%, 37.17% ± 1.72%, 37.78% ± 0.65%, 36.86% ± 1.23%, and 38.29% ± 3.72%. From the data in Figure 5, the degree of crystallinity increased as the number of FT cycles increased until reaching a saturation point after the first 3–5 FT cycles, as observed in previous work.[41] This result can be explained in that consecutive FT cycles build upon the foundation that was laid in creating the "knots" in the network during the first FT cycle.[51] The loosely-formed crystallites from the first FT cycle were continually developed due to further molecular chain aggregation with subsequent FT cycles, and the creation of new crystallites progresses until reaching a plateau.[1,45,46] In characterizing the changes to crystallinity with increasing number of FT cycles, it became evident to fix the number of FT cycles for continued tensile flaw and fatigue studies.

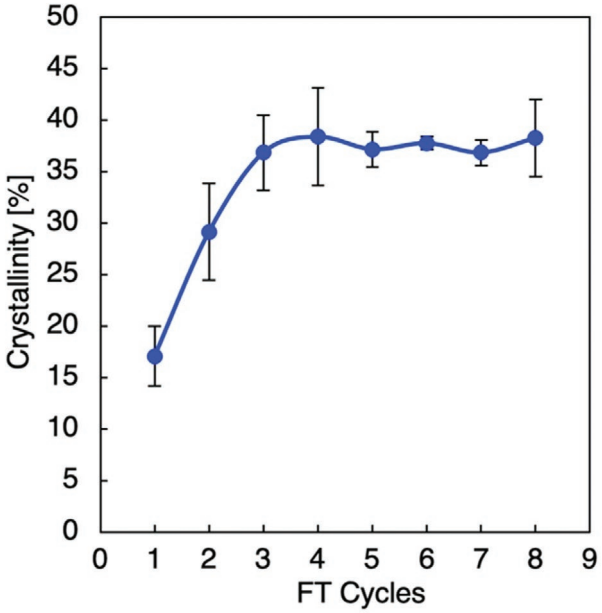

Figure 5. Crystallinity of PVA samples with varying numbers of FT cycles obtained from DSC measurements. Data depict mean crystallinity value ± standard deviation.

In terms of ease-of-processing concerns, the only sample that was difficult to remove from the mold due to insufficient mechanical stability was 1 FT cycle. Each cycle after that made the processing easier, with the only difference between FT cycles in terms of ease-of-processing was the amount of time it took for additional FT cycles. Based on the small difference between 3 and 4 FT in terms of ease-of-processing, the deciding factor for selecting an appropriate FT cycle number for subsequent mechanical testing came down to maximizing toughness. Since the 4 FT cycle sample had the largest toughness value, it was selected as the FT cycle number for further tensile study. In addition, the 2 FT cycle sample was selected for further tensile study due to its near matching of the toughness of the control sample in a prior PVA hydrogel study.[27]

2.4. Monotonic Mechanical Characterization of Samples with Macroscale Flaws

Using 4 and 2 FT samples as starting blocks, the next portion of this study set out to characterize the impact of two different macroscale flaw types on the tensile strength of the PVA hydrogel. The flaws utilized were 0.5, 1, 2, 3, and 4 mm sharp cracks as well as 0.5, 1, 2, 3, and 4 mm cylindrical holes. Tensile properties of the PVA hydrogel were analyzed using the customized sample shape depicted in Figure 2B for sharp cracks

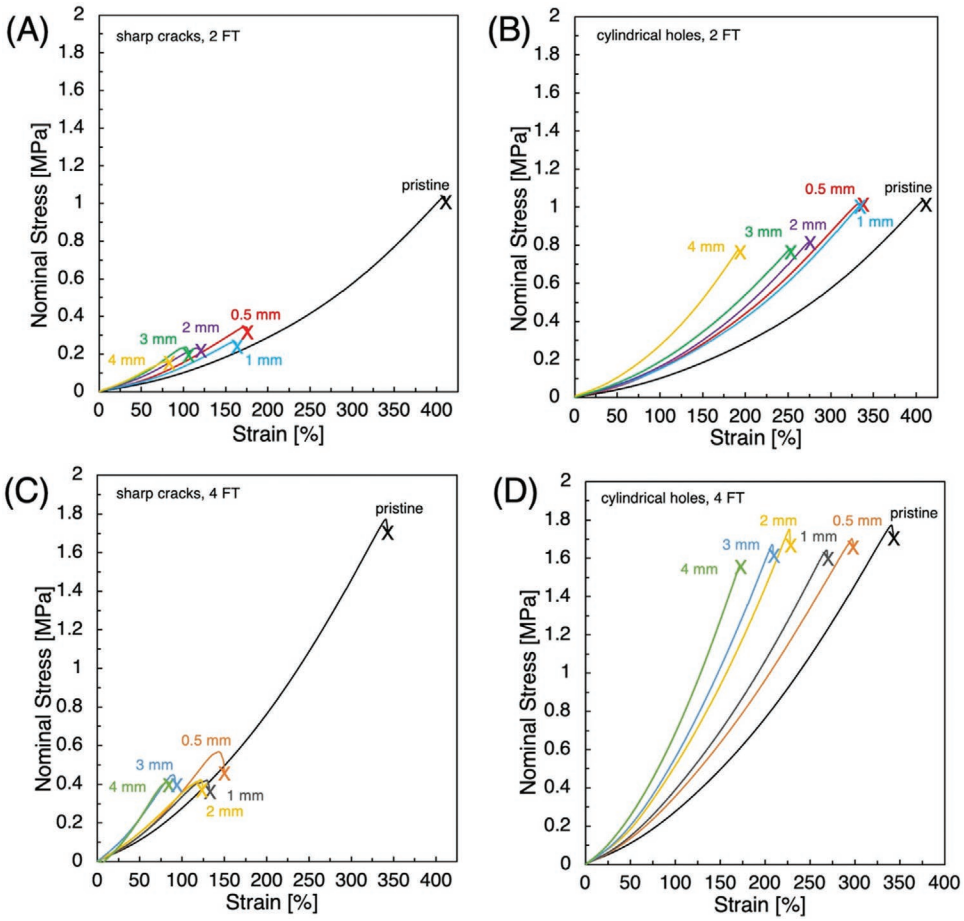

Figure 6. Nominal tensile stress–strain behavior for pristine, 0.5, 1, 2, 3, and 4 mm sharp crack 2 FT (A) and 4 FT (C) PVA samples, and pristine, 0.5, 1, 2, 3, and 4 mm cylindrical hole 2 FT (B) and 4 FT (D) PVA samples in monotonic tension for the customized, thicker fatigue sample shape.

and Figure 2C for cylindrical holes depending on the chosen hole diameter, with the testing rate remaining the same from the FT screening process at 15 mm min^{-1}. Further consideration of the introduction of flaw type during synthesis (before or after FT) may be considered in future work. The results of this testing for 2 FT cycles can be seen below in **Figure 6**A for sharp cracks and Figure 6B for cylindrical holes. Accordingly, the results of this testing for 4 FT cycles can be seen below in Figure 6C for sharp cracks and Figure 6D for cylindrical holes. The area used to calculate the stress values was the load-bearing area, taking into account the dimension of the given flaw. The force divided by the load-bearing area for these tests is called the "nominal stress", as provided on the y-axis.

In evaluating Figure 6, samples with a sharp crack experienced a significantly greater degree of ultimate tensile strength loss than those with a cylindrical hole. As the dimension of the flaw increased, the failure strain became smaller for both sharp crack and cylindrical hole samples. Samples that had undergone 4 FT cycles with cylindrical holes did not experience the same gradual decline in ultimate tensile strength as compared to samples that had undergone 2 FT cycles with cylindrical holes. The goal of comparing cylindrical hole and sharp crack in 2 and 4 FT cycles was to obtain a possible similarity in properties across different flaw types to investigate in tensile fatigue testing. As seen in Figure 6, the 0.5 mm sharp crack and 4 mm cylindrical hole have comparable failure strain values for both 2 and 4 FT cycles. In this way, tensile fatigue testing can be carried out in a displacement-controlled manner based on failure strain to compare the cylindrical hole and sharp crack across different FT cyclic processing steps. As a result, these two specific flaw types and dimensions (0.5 mm sharp crack and 4 mm cylindrical hole) were selected for completing tensile fatigue testing for the development of a fatigue life curve.

Two simple models were used to evaluate the losses in mechanical properties with flaws, one based on nominal stress (load-bearing area impact) and another based on fracture mechanics for a Modified Single Edge-Crack tension specimen, known as MSE(T).[26] For the purposes of this discussion, the terms "fracture mechanics", "stress intensity", and "Modified Single Edge-Crack tension" will be used interchangeably. The process of creating these two models can be found in the Experimental Section. Briefly, the nominal stress model simply considers a decrease in sample area to translate to a proportional drop in sample strength. This model gives way to an upper bound in predicting loss of strength in the presence of a flaw (i.e., smallest possible strength loss for a given flaw size). On the other hand, the fracture mechanics model gives way to a lower bound in predicting loss of strength in the presence of a

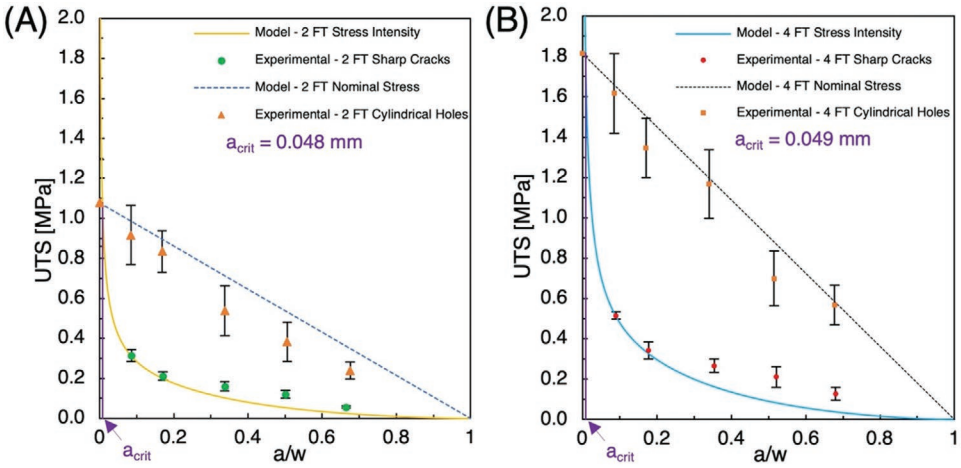

Figure 7. Comparison of experimental ultimate tensile strength with nominal stress and stress intensity models for varying cylindrical holes and sharp cracks for A) 2 FT and B) 4 FT cycle PVA samples. The x-axis a/w is defined as the ratio of the flaw size "a" to the width of the sample "w."

flaw (i.e., greatest possible strength loss for a given flaw size). Comparison of experimental ultimate tensile strengths (UTS) to these two models can be seen in **Figure 7**a for 2 FT cycles and Figure 7B for 4 FT cycles.

The results in Figure 7 highlight the extreme sensitivity of both 2 and 4 FT hydrogels toward the type of flaw despite the ability of the material to deform significantly and blunt flaw geometry. The experimental strength dropped dramatically for even the smallest sharp crack flaw of 0.5 mm. This large decrease was not observed in the cylindrical hole defect from pristine to 0.5 mm cylindrical hole. In observing these trends, the PVA hydrogels were far more sensitive to the crack-based flaw as opposed to the cylindrical hole-based flaw, as originally hypothesized and common for other much stiffer, non-hydrogel materials. The geometric shape change of the cylindrical hole-based flaw shows effective blunting in comparison to the intensification of local stresses at the tip of the crack-based flaw which blunts, but much less effectively. In addition, the data in Figure 7 confirmed an accurate deployment of the two extreme models. The stress intensity (fracture mechanics) model provided a lower bound of strength loss, while the nominal stress (load-bearing impact) model provided an upper bound of strength loss. The experimental data trend for crack-based flaws finished above the model due to the difficulty of perfectly ensuring the crack tip came to a sharp, geometrical point. This was unrealistic to provide a perfect crack tip, just as it would be in practical applications of sustaining such damage. The experimental data trend for the cylindrical hole-based flaws fell slightly below the predicted nominal stress model due to idealistic nature of the model. It accounted for pristine samples with no other defects present in order to show a proportional drop in strength from sample area, and this was difficult to ensure experimentally. The critical flaw size was determined from the intersection of the stress intensity model curve and nominal stress model curve. Assuming a 6 mm width for a sample, this value was 0.048 mm for 2 FT cycle samples and 0.049 mm for 4 FT cycle samples. As such, in theory, any flaw larger than about 50 micrometers would ensure rapid loss in ultimate tensile strength for the hydrogel samples at a rate much more significant than loss of load-bearing area. Flaws smaller than 50 micrometers would have, in theory, minimal impact on the hydrogel strength under monotonic loading.

2.5. Progression and Development of Flaw Type in Cyclic Tensile Testing

The remaining work of this study sought to characterize the progression and development of flaws under cyclic loading. As previously mentioned, the sensitivity of hydrogels toward a specific type of flaw is critical to understand what type of damage and how long will it take to lead to untimely failure. For this testing, PVA hydrogel samples were prepared with 2 and 4 FT cycles with 0.5 mm sharp cracks and 4 mm cylindrical hole-based flaws, respectively. The monotonic tensile data from Figure 7 was used to establish an average failure strain and subsequent standard deviation levels (minimum $n = 7$ tests for each flaw type and size). **Table 1** illustrates the target failure strain testing levels for 2 and 4 FT cycles of both cylindrical holes and sharp cracks.

Table 1. Target failure strain testing levels for PVA samples with 2 and 4 FT cycles with cylindrical holes and sharp cracks.

Sample Type	0.5σ	1σ	2σ	3σ
2 FT-0.5 mm sharp crack	175.10%	171.99%	165.79%	159.58%
2 FT-4 mm cylindrical hole	184.53%	171.24%	144.65%	118.05%
4 FT-0.5 mm sharp crack	149.65%	146.82%	141.16%	135.51%
4 FT-4 mm cylindrical hole	175.76%	166.24%	147.20%	128.16%

These flaw types were selected due to the similarity in their failure strain values, and they were tested in a strain-controlled manner at a constant strain rate of 2.6 s^{-1} based on the strain levels in Table 1. This strain rate was used in order to reduce the total time for each test with the assumption of samples lasting 100 000 cycles (runout samples). In addition, this strain rate aimed to prolong tensile loads before buckling of the sample became a more prominent effect in keeping the sample in a compressed state rather than a stretched one.[27] Both types of flaws for 2 and 4 FT samples had different monotonic failure strains as seen in Table 1. As a result, the testing amplitudes and frequencies had to be slightly adjusted for the applied strain rate of 2.6 s^{-1} to remain approximately constant across all tests.

Both the 2 and 4 FT systems were analyzed with four tests (n = 4) at four different standard deviations levels (0.5σ, 1.0σ, 2.0σ, and 3.0σ) to make for a total of 16 samples for each type of flaw (0.5 mm sharp crack and 4 mm cylindrical hole). Nominal stress versus strain over cyclic loads for 2 and 4 FT at one standard deviation level from the failure strain for both 0.5 mm crack and 4 mm cylindrical hole can be seen in Figure S2, Supporting Information. A plot of strain range versus cycles to failure can be seen in **Figure 8**A for 2 FT cycles and Figure 8B for 4 FT cycles.

As shown in Figure 8, cylindrical hole samples for both 2 and 4 FT cycles had more runout samples. Failure of a sample before 100 000 cycles was defined as a complete tear of the sample. Some cylindrical hole samples completed 100 000 cycles as a semicircle (i.e., one half of the circle had broken during the test, leaving the other half intact for the remainder of the test). However, this was not defined as failure of the sample due to part of the sample remaining. In addition, some crack-based samples from 2 and 4 FT experienced crack growth to varying degrees over the duration of the test. However, this damage accumulation was not considered a failure since complete tearing of the sample was not achieved. In this sense, the runout samples should not be considered "safe-life" endurance limit samples, where stresses below this result in no fatigue damage progression. Even the runout samples often had visible damage progression in terms of growing flaws.

The data shown in Figure 8 makes it difficult to ascertain sample performance across different failure strain testing levels with each flaw type. In order to fully characterize the results of fatigue testing, each sample was reviewed for the tensile nominal stress range experienced at the median time point of the test according to our previous work.[27] Median life tensile nominal stress range was defined as the maximum tensile nominal stress the sample experienced at the median time point of the test. In testing these samples in a strain-controlled manner with constant strain rate, tensile stresses must be invoked to compare samples with different failure strain values. As a result of the samples slightly buckling in the progression of a test, only tensile nominal stress at the median time point was considered instead of compressive ones brought on as the samples experienced stress relaxation. All samples were evaluated for their median life tensile nominal stress range, and the results of this analysis can be seen in **Figure 9**A for 2 FT samples and Figure 9B for 4 FT samples. The area used to calculate these tensile fatigue stress values was the load-bearing area, taking into account the dimension of the given flaw. The force divided by the load-bearing area for these tests is called the "median life tensile nominal stress range", as provided on the y-axis.

In comparing the median life tensile stress range of samples tested, it became clear that samples with much smaller 0.5 mm cracks performed worse than samples with much larger 4 mm cylindrical holes in stress-life space. Furthermore, the 0.5 mm sharp cracks that underwent 4 FT cycles outperformed the 0.5 mm sharp cracks that underwent 2 FT cycles. The same assertion can be made for 4 FT cylindrical holes with respect to 2 FT cylindrical holes. These trends from fatigue testing were consistent with the trends observed in monotonic tensile testing in Figure 6 which implies the increases in monotonic toughness translated to increases in fatigue strength. Tensile fatigue stress threshold was defined here as the largest median tensile nominal stress a sample had endured without failing completely. These values were: 0.1082 MPa for 2 FT-0.5 mm

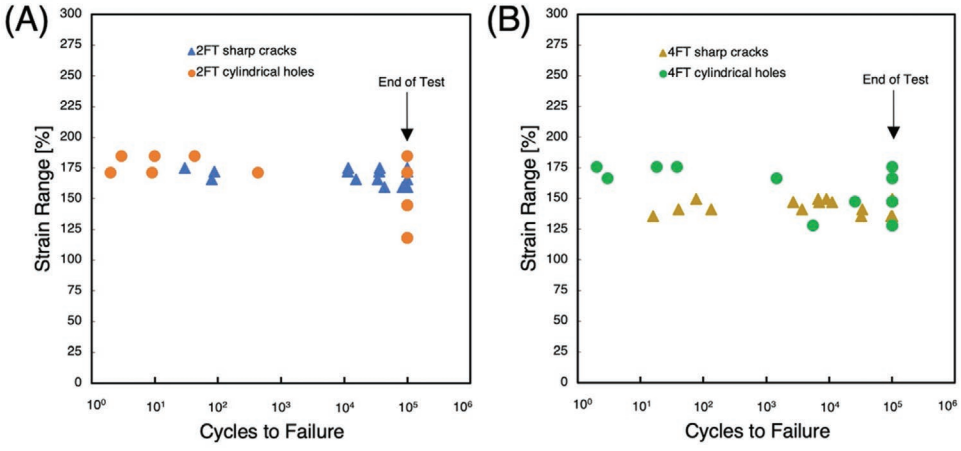

Figure 8. Tensile fatigue data for A) 2 FT and B) 4 FT PVA samples with sharp cracks and cylindrical holes based on strain range as a function of cycles to failure. A sample that lasted 100 000 cycles without failure is considered a "runout" sample with an arrow indicating its position in the graph. Four strain levels for both the cylindrical hole and sharp crack samples are utilized for 2 and 4 FT (0.5σ, 1.0σ, 2.0σ, and 3.0σ). Once 100 000 cycles are completed, the test is concluded.

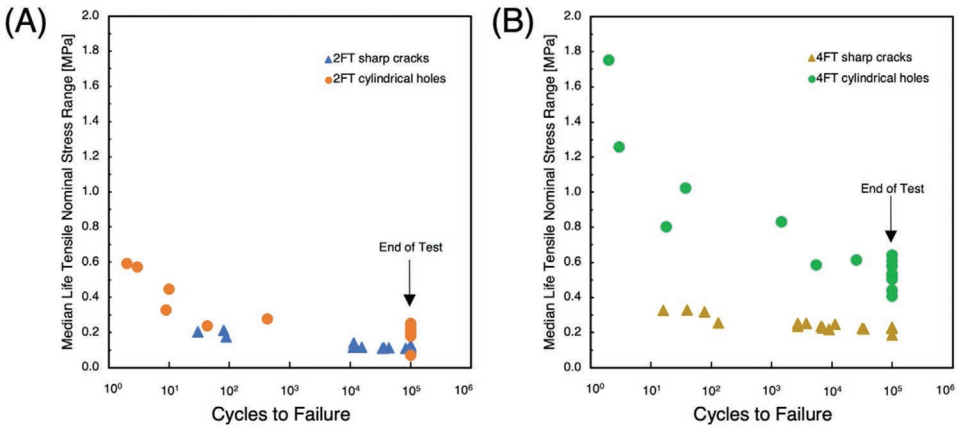

Figure 9. Tensile fatigue data for A) 2 FT and B) 4 FT PVA samples with sharp cracks and cylindrical holes based on median life tensile stress range as a function of cycles to failure. A sample that lasted 100 000 cycles without failure is considered a "runout" sample with an arrow indicating this position in the graph. A sample reaching 100 000 cycles marked the end of the test.

sharp crack, 0.2274 MPa for 2 FT-4 mm cylindrical hole, 0.1865 MPa for 4 FT-0.5 mm sharp crack, and 0.5812 MPa for 4 FT-4 mm cylindrical hole. Again, damage was still often progressing at these stress levels and with further cycling, the samples would likely fail so this stress threshold is not a classical "endurance limit". This fatigue data can be explained by considering the amplification of local stresses at the tip of a sharp crack. These local stresses were far more damaging than a cylindrical hole that did not have a site of extremely concentrated, amplified stress. The stresses in the cylindrical hole samples were more evenly distributed as opposed to the samples with a sharp crack. Although these effects are well known in the fatigue of harder materials, they have not been previously demonstrated in soft, wet hydrogels.

For a complete analysis of the impact of FT cyclic processing on monotonic and fatigue behavior, tensile stress values were analyzed across different sample shapes, flaw geometries, and testing types for both 2 and 4 FT cycles. Ultimate tensile strength was used for monotonic tensile testing, while median life tensile nominal stress range was utilized for tensile fatigue testing in this comparison of additional FT cyclic steps. These results are compiled in **Table 2**, including the percentage increase from 2 to 4 FT cycles.

In all cases, the samples experience an increase in tensile stress values when comparing 2 to 4 FT cycles. The greatest jumps in additional FT cyclic steps were realized for pristine-Type V shape-monotonic testing, 4 mm cylindrical hole-Fatigue shape-monotonic testing, and 4 mm cylindrical hole-Fatigue shape-fatigue testing. Furthermore, the stress values drop from those without defects and monotonic loading, to those with defects and monotonic loading, and finally to those with defects and fatigue loading. Moving forward, researchers must apply caution in exclusively evaluating increasing the strength/toughness of their hydrogels without giving attention to the impact of various defects and loading profiles (cyclic versus monotonic). In this study, the impact of increased toughness and strength was most significant when measured in a perfect, flaw-free sample. Samples with crack-like defects showed an increase in fatigue strength when monotonic toughness was increased, but not with the same relative quantitative impact.

In the realm of soft materials, this flaw analysis and subsequent fatigue examination are critical for understanding the initiation and progression of sustained damage toward untimely material failure. Often times, researchers seek to make flaw- or notch-insensitive hydrogels to show resistance to failure. In a practical sense, it is extremely difficult to prevent all types of damage from occurring. This relentless pursuit leaves a critical question for synthetic hydrogels with biomedical applications: What kind of damage is sustainable before it develops and progresses to long-term failure? Unfortunately, this pursuit of creating tough, flaw-insensitive hydrogels has created an enormous need in understanding the effects of unplanned,

Table 2. Comparison of tensile strength for different sample shapes, flaw geometries, and testing types for both 2 FT cycles and 4 FT cycles.

Sample Type	2 FT cycles [MPa]	4 FT cycles [MPa]	Percentage Increase [%]
No Flaw-Type V shape, Monotonic Testing, UTS	0.8042	2.3814	196.1
No Flaw-Custom Fatigue shape, Monotonic Testing, UTS	1.0781	1.8159	68.4
0.5 mm sharp crack-Custom Fatigue Shape, Monotonic Testing, UTS	0.3425	0.5664	65.3
4 mm cylindrical hole-Custom Fatigue Shape, Monotonic Testing, UTS	0.7399	1.7605	137.9
0.5 mm sharp crack-Custom Fatigue Shape, Fatigue Testing, Median Life Tensile Nominal Stress Range	0.1082	0.1865	72.3
4 mm cylindrical hole-Custom Fatigue Shape, Fatigue Testing, Median Life Tensile Nominal Stress Range	0.2274	0.5812	155.6

sustained damage with relation to long-term mechanical behavior. It has become essential to study the progression of different flaw types as it relates to fatigue properties to screen synthetic hydrogels for their suitability in biomedical applications. The nominal stress and stress intensity analysis created upper and lower bounds for the largest strength loss (sharp crack) and smallest strength loss (cylindrical hole). The fatigue study utilized in this work demonstrated that early failure of a synthetic hydrogel may come from flaws assumed to have no major impact and difficult to observe upon material synthesis. Hydrogels can only be trusted for long-term use if their resistance and response to flaws have been well-characterized across flaw types and cyclic loading regimes (low and high cycle fatigue).

In conclusion, PVA hydrogels present an excellent model system to understand the progression of flaws as it relates to long-term mechanical behavior. In further characterizing soft materials of similar tunable mechanical properties, PVA hydrogels provide a strong foundation for advanced tensile study for even more biomedical applications. High-level control over the mechanical properties was attained via control over the FT cyclic processing steps to maximize toughness. This work set out to characterize the fatigue behavior of PVA-based hydrogels with different flaw types of sharp cracks and cylindrical holes. A screening process of a hydrogel's toughness was employed, and it was highly dependent on the number of FT cycles. The swelling ratio and crystallinity of samples were also contingent upon the same FT cyclic process. The shape of the prepared hydrogels was adjusted to accommodate for a larger range of possible dimensions for flaws from 0.5 to 4 mm. Two models were created to account for the strength loss of a hydrogel sample based on its given type (sharp crack or cylindrical hole) and size. Flaws of controlled dimension were then used for tensile fatigue testing to understand progression of damage toward early sample failure. Hydrogel specimens with a sharp crack of 0.5 mm and cylindrical hole of 4 mm were employed in tensile fatigue testing to generate the strain range curve and subsequent median life tensile nominal stress range curve. As a result of these tests, it was concluded that additional FT cycles improved fatigue behavior from 2 to 4 FT. In addition, the sharp 0.5 mm cracks for both 2 and 4 FT performed poorly in comparison to their 4 mm cylindrical hole counterparts. The cyclic, tensile portion of this study aimed to shed light on the importance of characterizing flaw behavior as it relates to long-term use of soft materials in biomedical applications.

3. Experimental Section

Materials: The PVA (molecular weight (M_w) 85 000–124 000 Da, 99+% hydrolyzed) in this study was used without further purification and purchased from Sigma-Aldrich, St. Louis, MO, USA. Deionized water used in this study was supplied from a Pureflow Inc. Portable Exchange Type II system. Stainless steel dowel pins were acquired from McMaster Carr, Atlanta, GA, USA and Amazon.com, Inc., Seattle, WA, USA. A razor blade was used to create sharp cracks of specified lengths.

Material Preparation: For preparation of PVA hydrogel samples, (9.518 g) PVA was combined with deionized water (50 mL) in 100 mL round bottom flask. This mixture was sealed with a rubber septum, and it was heated and stirred for a minimum of 3 h at 95 °C in an oil bath until the PVA was fully dissolved to form a homogenous solution. Once fully dissolved, the resulting solution was then removed from the 95 °C oil bath and sonicated for roughly 30 s to 1 min to remove any bubbles close to the surface. The hot solution was then poured into stainless-steel molds that matched the dimensions of the ASTM D638-14 Type V shape for monotonic tensile testing, swelling studies, and DSC characterization.[52] Fatigue tensile specimens were prepared in the same manner in a customized, stainless-steel mold that had a thicker gauge section. The hot solution was poured into the mold, parafilm was utilized to cover the mold, and tape was used over the top of the parafilm to create a sufficient seal. For fatigue samples with controlled cylindrical defects, a metal hollow punch was used to create a hole in the parafilm that aligned with the center of the gauge section. The hot solution would be poured into the mold with the parafilm placed on top. Next, stainless-steel dowel pins of varying diameters were placed into the hole of the parafilm for each sample, and tape was placed over the top of the pin. For example, a 1.5 mm hollow punch was used for a 2 mm cylindrical defect to create a sufficient seal around the stainless-steel pin. Stainless-steel dowel pins were utilized as purchased. When FT cyclic processing was complete, pins were easily removed from the gauge section of the hydrogel to create cylindrical holes of controlled diameters. For fatigue samples with controlled sharp crack defects, a razor blade was used to create this crack once FT cyclic processing was complete. The molds were frozen at −23 °C for 20 h followed by 4 h of thawing at 20 °C to complete one FT cycle (1 FT). This freezing and subsequent thawing process was repeated for 2 through 8 FT cycles (2 through 8 FT). Depending on the number of FT cycles employed, the samples were easily removed from the stainless-steel molds using a spatula and characterized for their properties. Type V samples and fatigue samples were stored in deionized water until monotonic or fatigue tensile testing and DSC characterization had occurred.

Mechanical Testing: Monotonic tensile measurements were carried out using a 50-lb load cell on either an Instron 1321 (Instron, Norwood, MA, USA) instrument or a TestResources 830 (TestResources, Shakopee, MN, USA) load frame. Comparison of monotonic tensile toughness results was completed with one-way analysis of variance (ANOVA); α = 5%; * depicts statistical significance in the following manner: $*p < 0.05$; $**p < 0.01$, $***p < 0.001$, $****p < 0.0001$. All fatigue tests were completed on the Instron 1321, while an extensometer was used to determine an experimental effective length for both monotonic and fatigue samples on the TestResources 830 load frame with a 50-lb load cell. Monotonic tension samples were prepared from an ASTM D638-14 Type V shape, tested at a rate of 0.25 mm sec^{-1}, and led to the compilation of results from corresponding individual stress–strain curves. Once the screening process of the FT cycles in the Type V shape was complete, the thicker fatigue-shaped samples were tested for monotonic tensile comparison with sharp cracks of controlled lengths (0.5, 1, 2, 3, and 4 mm) and cylindrical holes of controlled diameters (0.5, 1, 2, 3, and 4 mm) at a rate of 0.25 mm sec^{-1}. For the purposes of discussion, the term "cut" is interchangeable with "sharp crack." Fatigue samples were prepared from a customized shape in order to characterize larger flaw sizes as well as prevention of sample buckling during cyclic tests. A tap water bath at 37 °C was used to prevent samples from drying out during cyclic testing of fatigue samples.

Upon analyzing these tests with respect to nominal stress and stress intensity models (see Stress Intensity Model and Nominal Stress Model in later Experimental Sections), this study shifted focus to the progression and development of both flaw types as it related to long-term, cyclic testing. To compare materials of similar properties across different flaws of 2 and 4 FT cycles, Figure 6 was consulted. It was determined that similar failure strain values for 0.5 mm sharp crack and 4 mm cylindrical hole would provide the best comparison under similar testing conditions. As such, there became four distinct combinations to be tested: 0.5 mm sharp crack of 2 FT cycles, 0.5 mm sharp crack of 4 FT cycles, 4 mm cylindrical hole of 2 FT cycles, and 4 mm cylindrical hole of 4 FT cycles. For the fatigue analysis of both the 2 and 4 FT samples, a strain rate of 2.61 s^{-1} was utilized in order to retain prolonged tensile loads before buckling of the sample became a dominating effect as determined in the previous work.[27] The 0.5 mm sharp crack and 4 mm

cylindrical hole had slightly different monotonic failure strains, which ultimately led to adjusting the testing amplitudes and frequencies in order for the applied strain rate to remain constant across all tests. With all distinct testing combinations mentioned previously, it was decided to conduct $n = 4$ tests at each of the standard deviation levels (0.5σ, 1σ, 2σ, and 3σ) for a total of 16 samples for each combination.

Hydrogel Swelling: The ability of all FT cycles to uptake water was measured by recording the mass variation of the hydrogels after swelling in a 15 mL centrifuge tube of deionized water (12 mL) at room temperature for 24 h. Samples were prepared in the ASTM D638-14 Type V shape. Excess water on the external surface of the hydrogels was removed by lightly tapping the samples on a piece of filter paper. The samples were then weighed and subsequently dried to constant weight at 80 °C for 20 h in a Yamato drying oven. The ratio of the swollen weight to the dry weight was used to calculate a swelling ratio, q, below. The swelling ratio (q) of the hydrogel samples was defined as the ratio of the weight of swollen sample (W_s, swollen in deionized water for 24 h) divided by the weight of the fully dried-out sample (W_d, dried out at 80 °C for 20 h to constant weight) in Equation (2).

$$q = \frac{W_s}{W_d} \tag{2}$$

Each reported swelling ratio is an average of three parallel measurements.

Differential Scanning Calorimetry (DSC): All FT cycles were characterized for their crystallinity via DSC measurements on a Discovery DSC (TA Instruments, New Castle, DE, USA). Hydrogel samples were prepared in the ASTM D638-14 Type V shape. For each analysis, the hydrogel sample (about 5 to 7 mg) was placed into a Tzero aluminum pan with a flat Tzero lid pressed into place. The following protocol for DSC measurements was used: equilibrate to 40 °C, isotherm for 1 min, ramp 10 °C min^{-1} to 250 °C, isotherm for 3 min, ramp 10 °C min^{-1} to 40 °C, isotherm for 3 min, ramp 10°C min^{-1} to 250 °C, isotherm for 3 min, and ramp 10 °C min^{-1} to 40 °C. The percent crystallinity was calculated from the first heating curve in order to be representative of the FT procedure that the sample underwent before DSC analysis. DSC scans were repeated on fresh samples for a minimum of $n = 4$ for each FT cycle.

Stress Intensity Model: All samples tested were in the thicker, customized fatigue shape for 2 and 4 FT cycles. Monotonic tensile testing according to *Mechanical Testing* was employed to establish the tensile strength values. As for terminology, a was defined as the length of the crack, h was defined as the height of the sample's gauge section, and w was defined as the width of the sample's gauge section. The x-axis of modeling and experimental data was simply a ratio of the crack length, a, to the width of the sample gauge section, w. For creation of the modeling data, the non-dimensional geometric correction factor, β, was used as defined according to Equation (5) of Hammond et al.[26] This correction factor was calculated for each individual sample of both 2 and 4 FT (minimum $n = 7$) for a sharp crack of 0.5 mm (the smallest crack dimension that could be reliably reproduced with a razor blade). In the same manner as Equation (1) of Hammond et al.,[26] the stress value σ was also calculated based on the applied tensile load, thickness of the sample, and width of the sample (independent of the crack length).[26] In combination with the σ values, the β values were then used to calculate a K_i, or stress intensity factor, according to Equation (2) of Hammond et al. for each 0.5 mm crack-based sample.[26] An average K_i value was established among the samples for 2 FT cycles ($K_i = 0.467$ MPa $mm^{1/2}$) and 4 FT cycles ($K_i = 0.789$ MPa $mm^{1/2}$).

Once calculated, the K_i values for 2 and 4 FT, respectively, were held constant in order to create a new β value from systematically varying values of crack length a (from 0.01 to 6 mm) and holding the width w at a constant value of 6 mm. In this way, a new stress value could be obtained via the constant K_i value, constant w value, and unique β value based on the particular selection of crack length a (as observed in Equation (2) of Hammond et al).[26] These stress values were plotted against the ratio of the selected a value to constant w value (6 mm) to establish the stress intensity model. Experimental stress values were based on the area of the sample with the assumption of no crack present (i.e., height × width independent of crack length). These results were plotted against the ratio of the measured crack length a to the measured width w. Error bars were included to express the standard deviation value for each experimental tensile strength value.

Nominal Stress Model: All samples tested were in the thicker, customized fatigue shape for 2 and 4 FT cycles. Monotonic tensile testing according to *Mechanical Testing* was employed to establish the tensile strength values. As for terminology in this model, a was defined as the diameter of the cylindrical hole, h was defined as the height of the sample's gauge section, and w was defined as the width of the sample's gauge section. The x-axis of modeling and experimental data was simply a ratio of the cylindrical hole diameter, a, to the width of the sample gauge section, w. For both modeling and experimental data, stress was calculated based on the area of the sample with the assumption of no cylindrical defect present (i.e., height × width independent of cylindrical hole diameter). Model data was established by taking the average ultimate tensile strength of a sample with no defect present (i.e., at y-axis intercept) as a data point. A line was then fitted from this data point to the x-axis intercept, establishing the model. Essentially, this model was created from the idea that a decrease in sample area meant a proportional decrease in sample strength.

The experimental stress data compared to this model was calculated in the same manner independent of the cylindrical hole diameter. The average ultimate tensile stress was computed for 0.5, 1, 2, 3, and 4 mm cylindrical holes. These results were plotted against the ratio of the measured diameter a to the measured width w. The critical flaw size, a_{crit}, was determined to be the intersection of the stress intensity model with the nominal stress model. In this sense, a sample with a flaw size below the value of a_{crit} was predicted to have no impact on the sample's strength. Any sample with flaw larger than a_{crit} was sensitive to the particular flaw type and dimension. Error bars were included to express the standard deviation value for each experimental tensile strength value.

Acknowledgements

The authors gratefully acknowledge Patrick McGuire, John Goodfellow, Bernard Jelinek, and Richard Nappi for technical assistance. Financial support of Duke University is acknowledged.

Conflict of Interest

The authors declare no conflict of interest.

Keywords

defects, tensile fatigue, fracture mechanics, hydrogels, soft materials

Received: November 2, 2020
Revised: November 26, 2020
Published online: December 21, 2020

[1] P. Yusong, D. Jie, C. Yan, S. Qianqian, *Materials Technology* **2016**, *31*, 266.
[2] G. Tao, Y. Wang, R. Cai, H. Chang, K. Song, H. Zuo, P. Zhao, Q. Xia, H. He, *Mater. Sci. Eng., C* **2019**, *101*, 341.
[3] A. S. Oliveira, S. Schweizer, P. Nolasco, I. Barahona, J. Saraiva, R. Colaço, A. P. Serro, *Lubricants* **2020**, *8*, 36.

[4] W. Li, D. Wang, W. Yang, Y. Song, *RSC Adv.* **2016**, *6*, 20166.
[5] S. Jiang, S. Liu, W. Feng, *J. Mech. Behav. Biomed. Mater.* **2011**, *4*, 1228.
[6] W. Święszkowski, D. N. Ku, H. E. N. Bersee, K. J. Kurzydlowski, *Biomaterials* **2006**, *27*, 1534.
[7] C. M. Hassan, N. Peppas, *Adv. Polym. Sci.* **2000**, *153*, 37.
[8] M. Oka, T. Noguchi, P. Kumar, K. Ikeuchi, T. Yamamuro, S. H. Hyon, Y. Ikada, *Clin. Mater.* **1990**, *6*, 361.
[9] J. A. Stammen, S. Williams, D. N. Ku, R. E. Guldberg, *Biomaterials* **2001**, *22*, 799.
[10] A. Takasu, K. Aoi, M. Tsuchiya, M. Okada, *J. Appl. Polym. Sci.* **1999**, *73*, 1171.
[11] Y. Jiang, A. Schädlich, E. Amado, C. Weis, E. Odermatt, K. Mäder, J. Kressler, *J. Biomed. Mater. Res., Part B* **2010**, *93B*, 275.
[12] M. Kobayashi, Y.-S. Chang, M. Oka, *Biomaterials* **2005**, *26*, 3243.
[13] R. Ricciardi, F. Auriemma, C. De Rosa, F. Lauprêtre, *Macromolecules* **2004**, *37*, 1921.
[14] Q. Su, Y. Wang, S. Guan, H. Zhang, G. H. Gao, X. Zhu, *RSC Adv.* **2016**, *6*, 30570.
[15] J. Ma, J. Lee, S. S. Han, K. H. Oh, K. T. Nam, J.-Y. Sun, *ACS Appl. Mater. Interfaces* **2016**, *8*, 29220.
[16] R. Zhang, L. Wang, Z. Shen, M. Li, X. Guo, Y. Yao, *Macromol. Rapid Commun.* **2017**, *38*, 1700455.
[17] G. Du, F. Wu, Y. Cong, L. Nie, S. Liu, G. Gao, J. Fu, *Chem. Commun.* **2015**, *51*, 15534.
[18] Y. Wang, J. Wu, Z. Cao, C. Ma, Q. Tong, J. Li, H. Liu, J. Zheng, G. Huang, *Polymer* **2019**, *179*, 121661.
[19] M. Sun, J. Qiu, C. Lu, S. Jin, G. Zhang, E. Sakai, *Polymers* **2020**, *12*, 2263.
[20] E. Zhang, R. Bai, X. P. Morelle, Z. Suo, *Soft Matter* **2018**, *14*, 3563.
[21] C. Chen, Z. Wang, Z. Suo, *Extreme Mechanics Letters* **2017**, *10*, 50.
[22] W. Zhang, J. Hu, J. Tang, Z. Wang, J. Wang, T. Lu, Z. Suo, *ACS Macro Lett.* **2019**, *8*, 17.
[23] R. Long, C.-Y. Hui, *Soft Matter* **2016**, *12*, 8069.
[24] F. Wang, R. A. Weiss, *Macromolecules* **2018**, *51*, 7386.
[25] T. Stegmaier, P. Schneider, A. Vohrer, H. Planck, R. Blum, H. Bögner-Balz, in *Textiles, Polymers and Composites for Buildings*, (Ed: G. Pohl), Woodhead Publishing, Cambridge **2010**, pp. 129–191e.
[26] M. J. Hammond, S. A. Fawaz, *Eng. Fract. Mech.* **2016**, *153*, 25.
[27] W. J. Koshut, D. Smoot, C. Rummel, A. Kirillova, K. Gall, *Macromol. Mater. Eng.* **2020**, *305*, 1900784.
[28] C. M. Hassan, N. A. Peppas, *Macromolecules* **2000**, *33*, 2472.
[29] S. R. Stauffer, N. A. Peppast, *Polymer* **1992**, *33*, 3932.
[30] Z. Gong, G. Zhang, X. Zeng, J. Li, G. Li, W. Huang, R. Sun, C. Wong, *ACS Appl. Mater. Interfaces* **2016**, *8*, 24030.
[31] Y. Deng, M. Huang, D. Sun, Y. Hou, Y. Li, T. Dong, X. Wang, L. Zhang, W. Yang, *ACS Appl. Mater. Interfaces* **2018**, *10*, 37544.
[32] H. Fan, J. Wang, Z. Jin, *Macromolecules* **2018**, *51*, 1696.
[33] T. Chen, Y. Chen, H. U. Rehman, Z. Chen, Z. Yang, M. Wang, H. Li, H. Liu, *ACS Appl. Mater. Interfaces* **2018**, *10*, 33523.
[34] H. Zhi, X. Fei, J. Tian, L. Zhao, H. Zhang, M. Jing, L. Xu, Y. Wang, Y. Li, *Biomater. Sci.* **2018**, *6*, 2320.
[35] M. T. Haseeb, M. A. Hussain, S. H. Yuk, S. Bashir, M. Nauman, *Carbohydr. Polym.* **2016**, *136*, 750.
[36] N. D. Broom, A. Oloyede, *Biomaterials* **1998**, *19*, 1179.
[37] Y. Shi, D. Xiong, Y. Liu, N. Wang, X. Zhao, *Mater. Sci. Eng., C* **2016**, *65*, 172.
[38] U. Fumio, Y. Hiroshi, N. Kumiko, N. Sachihiko, S. Kenji, M. Yasunori, *Int. J. Pharm.* **1990**, *58*, 135.
[39] J. Tavakoli, J. Gascooke, N. Xie, B. Z. Tang, Y. Tang, *ACS Appl. Polym. Mater.* **2019**, *1*, 1390.
[40] Y. Pan, *Micro Nano Lett.* **2010**, *5*, 237.
[41] R. Ricciardi, F. Auriemma, C. Gaillet, C. De Rosa, F. Lauprêtre, *Macromolecules* **2004**, *37*, 9510.
[42] R. C. Simoni, G. F. Lemes, S. Fialho, O. H. Gonçalves, A. M. Gozzo, V. Chiaradia, C. Sayer, M. A. Shirai, F. V. Leimann, *An. Acad. Bras. Cienc.* **2017**, *89*, 745.
[43] V. R. Patel, M. M. Amiji, *Pharm. Res.* **1996**, *13*, 588.
[44] A. Suzuki, S. Sasaki, *Proc. Inst. Mech. Eng., Part H* **2015**, *229*, 828.
[45] T. Hatakeyema, J. Uno, C. Yamada, A. Kishi, H. Hatakeyama, *Thermochim. Acta* **2005**, *431*, 144.
[46] J. L. Holloway, A. M. Lowman, G. R. Palmese, *Soft Matter* **2012**, *9*, 826.
[47] V. I. Lozinsky, L. G. Damshkaln, I. N. Kurochkin, I. I. Kurochkin, *Colloid J.* **2008**, *70*, 189.
[48] L. M. Sanchez, V. A. Alvarez, R. P. Ollier, *J. Appl. Polym. Sci.* **2019**, *136*, 47663.
[49] C.-M. Tang, Y.-H. Tian, S.-H. Hsu, *Materials* **2015**, *8*, 4895.
[50] A. M. Neres Santos, A. P. Duarte Moreira, C. W. Piler Carvalho, R. Luchese, E. Ribeiro, G. B. McGuinness, M. Fernandes Mendes, R. Nunes Oliveira, *Materials* **2019**, *12*, 559.
[51] F. Yokoyama, I. Masada, K. Shimamura, T. Ikawa, K. Monobe, *Colloid Polym. Sci.* **1986**, *264*, 595.
[52] ASTM D638-14, *Standard Test Method for Tensile Properties of Plastics*, ASTM International, West Conshohocken, PA, **2014**.